The 2010 IEEE/RSJ International Conference on
Intelligent Robots and Systems
October 18-22, 2010, Taipei, Taiwan

Two-Dimensional Needle Steering with a "Programmable Bevel" Inspired by Nature: Modeling Preliminaries

Seong Young Ko, *Member, IEEE*, Brian L. Davies, and Ferdinando Rodriguez y Baena, *Member, IEEE*

***Abstract*— Percutaneous interventions have attracted significant interest in recent years, but most approaches still rely on straight line trajectories between an entry site and a soft tissue target. Thus, to this day, a flexible probe able to bend along predefined curvilinear trajectories within a highly compliant medium without buckling is still an open research challenge. In this paper, we describe the concept of a "programmable bevel" tip, which is inspired by the ovipositor of certain wasps: the offset between two parts of a probe determines the steering direction of the tip thanks to a set of bevels included at the tip of each segment. A kinematic model of the flexible probe and programmable bevel arrangement is derived. Several parameters of the kinematic model are calibrated experimentally using our first prototype of the flexible probe, codenamed STING. Open- (feed-forward) and closed-loop (feedback) control strategies are then derived and implemented in simulation using the chained form representation, originally developed to control car-like robots. Simulated results demonstrate accurate two-dimensional needle steering in the presence of velocity, position, and initial posture disturbances.**

I. Introduction

Percutaneous intervention has always attracted significant interests because it is performed through a very small port in the skin [1]. For instance, tumor biopsy, brachytherapy, deep brain stimulation and localized drug delivery currently benefit from this operative technique to reduce tissue trauma and reduce hospitalization time.

If the lesion is reachable through a straight path, a straight rigid needle can be used. When a straight path does not seem possible or is not safe, a steerable needle can be utilized to reach a target while avoiding 'no-go' areas. With a flexible needle, however, localization of the tip position becomes more difficult because it is no longer possible to extrapolate tip position from a base measurement.

Consequently, there have been several approaches to the modeling of flexible needle behavior in soft tissue. DiMaio and Salcudean [2] and Glozman and Shoham [3] modeled the deflection of a thin needle as a function of tissue deformation to steer the tip around predefined obstacles in the plane of insertion by applying a suitable moment at the needle base. An alternative approach, which has been exploited by several research groups over the past few years, centers upon the unique steering capabilities of a very thin needle with bevel tip. Webster III *et al.* first proposed a kinematic model of the beveled tip needle to describe its behavior in soft tissue [4]. Alterovitz *et al.* then derived a motion-planning algorithm under uncertainty to obtain better targeting accuracy [5]. Reed *et al.* modeled the torsional dynamics of a flexible needle to analyze torsional behavior during needle insertion [6]. These studies have predominantly focused on open-loop trajectory following, which is effective in situations when appropriate models of the environment (i.e. the surrounding tissue), the needle, and their interaction can be obtained.

In the presence of significant uncertainty, for instance that introduced by the complex deformations of a soft tissue under a dynamic load, feedback control is required to guarantee performance. Kallem and Cowan proposed a plane alignment control algorithm for needle steering [7]. They utilized a stereo camera to measure the tip position of a needle and implemented a full-state observer to estimate other states. As a method to change the curvature of a thin and flexible needle, Minhas *et al*. proposed a duty-cycling spinning algorithm [8].

In the area of closed loop control of flexible needles, to our knowledge, only two demonstrations with image-guided feedback control are reported in the literature. Glozman and Shoham closed the control loop in their original approach [3] by means of fluoroscopic images, which were used to measure needle deflection during the insertion process [9]. Also, Reed *et al.* implemented an "on-off" controller based on stereo video cameras, which modifies the trajectory to a predefined target (through "bevel right" and "bevel left" commands) in response to instantaneous measurements of tip position [10].

Within this context, we are currently developing a bio-inspired flexible probe [11], which can alter its direction by means of a "*programmable bevel tip"* that will incorporate a small electromagnetic (EM) position sensor with up to six degrees of freedom of positional information. With this approach, closed loop control of the probe tip along an arbitrary trajectory can thus be achieved without the need for an external imaging system.

This paper described the kinematic modeling of the probe and a two-dimensional needle steering feedback control algorithm, which is validated here in simulation and is currently undergoing experimental trials on a first prototype. Specifically, Section II explains the concept of "programmable bevel" and presents the kinematic model of

Manuscript received March 5, 2010. This work was supported by the EU-FP7 Project ROBOCAST.

S. Y. Ko is with Department of Mechanical Engineering, Imperial College London, SW7 2AZ, UK (e-mail: s.ko@imperial.ac.uk).

B. L. Davies is with Department of Mechanical Engineering, Imperial College London, UK and the Italian Institute of Technology, Genova, Italy (e-mail: b.davies@imperial.ac.uk).

F. Rodriguez y Baena is with Department of Mechanical Engineering and the Institute of Biomedical Engineering, Imperial College London, SW7 2AZ, UK (corresponding author to provide phone: +44-(0)20-7594-7046; fax: +44-(0)20-7594-1472; e-mail: f.rodriguez@imperial.ac.uk).

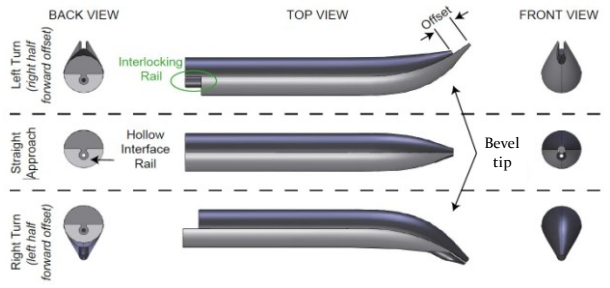

Fig. 1. Programmable bevel tip concept: the offset between two interlocked segments of a flexible probe determines the steering direction of the tip.

the probe and bevel assembly. Two-dimensional needle steering based on the kinematic model is explained in Section III. In Section IV, calibration methods to obtain important parameters of the kinematic model are described. Simulation results are summarized in Section IV, while a discussion of the simulation follows in Section V. Finally, conclusions and future work are outlined in Section VI.

II. "Programmable Bevel" Concept

A. Bio-Inspired Programmable Bevel

Our flexible probe was inspired by the ovipositor of the wood wasp, *Sirex noctilio*. The ovipositor is used to penetrate the bark of wood to deliver eggs through a long and hollow inner channel along its length. The ovipositor consists of several (two in the case of *Sirex noctilio*) valves, which are connected to each other by means of a special interlocking mechanism.

Based on this unique biological design and that of other ovipositor assemblies, where the insertion angle is controlled by the offset between valves, the concept of a "programmable bevel" is proposed here, which is illustrated in Fig. 1. The probe insertion direction is a function of the offset between probe segments, which are connected by means of a specially designed dovetail-shaped interlock [12]. Each segment is controlled by a corresponding linear actuator, which is connected to the proximal end and enables independent forward and backward sliding motion of each segment with respect to the other.

B. Kinematic Modeling

In this paper we assume that trajectories are defined in a plane and that the probe is aligned with the plane during initial setup. Therefore, the kinematic model of the probe is currently dealt with in two-dimensional space. Webster III *et al.* showed that the kinematic model of a thin beveled tip needle could be considered similar to that of a bicycle model with a fixed steering angle [4]. In the case of our probe, the steering direction can be altered using the offset between the two halves (segments) and the kinematic model can thus be considered to be similar to that of a bicycle able to steer. Fig. 2a shows the notation adopted to describe the flexible probe, while Fig. 2b shows the notation associated to a conventional bicycle model. If the origin of the bicycle model is chosen at the center of the rear wheel (P_b), its kinematic model is expressed as in (1), where x, y, θ, and φ indicate the x-axis and y-axis coordinates, the approach angle, and the steering angle of the bicycle model, respectively. In (1), v_1, v_2, and L indicate the forward velocity of a bicycle's body, the rate of change of steering angle, and the distance between the front and a rear wheels, respectively.

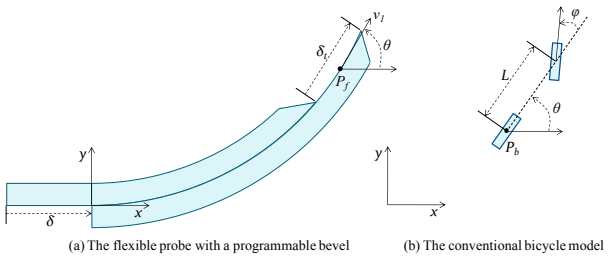

(a) The flexible probe with a programmable bevel (b) The conventional bicycle model

Fig. 2. Notation comparison between our flexible probe and conventional bicycle model.

$$\begin{bmatrix}\dot{x}\\ \dot{y}\\ \dot{\theta}\\ \dot{\varphi}\end{bmatrix}=\begin{bmatrix}\cos\theta\\ \sin\theta\\ \tan\varphi/L\\ 0\end{bmatrix}v_1+\begin{bmatrix}0\\0\\0\\1\end{bmatrix}v_2 \tag{1}$$

In (1), the relationship between the forward velocity (v_1) and the rotational velocity ($\dot{\theta}$) determines the instantaneous curvature (ρ) of a real trajectory [7] and it is a function of the steering angle (φ). In contrast to the bicycle model, however, in our probe the instantaneous curvature is assumed to be a function of the *steering offset* (δ_t) at the tip of the probe, as in (2), where $f(\delta_t)$ is a monotonically increasing function of the steering offset. In this research, we simplify the definition of $f(\delta_t)$ by treating the curvature (ρ) as being proportional to the steering offset, with a coefficient κ (mm^{-2}), based on preliminary experiments, as explained in Section IV-A. The kinematic model thus becomes as in (3), where v_1 and v_{t2} indicate the forward velocity and the rate of change of steering offset respectively.

$$\rho = f(\delta_t) \equiv \kappa\delta_t \tag{2}$$

$$\begin{bmatrix}\dot{x}\\ \dot{y}\\ \dot{\theta}\\ \dot{\delta}_t\end{bmatrix}=\begin{bmatrix}\cos\theta\\ \sin\theta\\ \kappa\delta_t\\ 0\end{bmatrix}v_1+\begin{bmatrix}0\\0\\0\\1\end{bmatrix}v_{t2} \tag{3}$$

The steering offset will be different if measured at the base rather than the tip of the probe, due to a number of factors associated with this mechanism of motion e.g. compressive and tensile deformation, probe body configuration and friction. Thus, let δ describe the offset between the two segments of the probe, as illustrated in Fig. 2, while δ_t describes the corresponding offset, measured at the tip of the probe. Disregarding material deformation, a relationship between the two offsets which takes into account the probe's configuration can be derived as follows. Considering a small segment of the flexible probe of length ds, as shown in Fig. 3, the curvature of the segment is $1/R_c$ and the distance to a

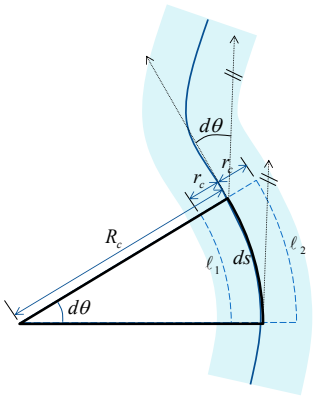

Fig. 3. Short segment of the flexible probe having two valves.

neutral axis for each segment is r_c. The length of each segment can be expressed as in (4). Given a segment with length ds, the angular difference between the two ends of the segment is $d\theta$, as in (5), and the difference between the two halves becomes $d\delta$, as in (6). By integrating both sides of (6), a relationship between $\Delta\delta$ and the approach angle θ (7), where ε (mm) is the distance between the neutral axes of the two segments, can be obtained. Assuming that the initial insertion direction for the probe is parallel to the x-axis, (i.e. $\theta_0 = 0$), the compensation amount is thus only proportional to the current tip direction of the probe.

$$\begin{aligned} \ell_1 &= (R_c - r_c)d\theta \\ \ell_2 &= (R_c + r_c)d\theta \end{aligned} \tag{4}$$

$$d\theta = ds / R_c \tag{5}$$

$$\begin{aligned} d\delta &= \ell_2 - \ell_1 = (R_c + r_c)d\theta - (R_c - r_c)d\theta \\ d\delta &= 2r_c d\theta = \varepsilon d\theta \end{aligned} \tag{6}$$

$$\Delta\delta = \varepsilon\,\Delta\theta = \varepsilon\,(\theta - \theta_0) \equiv \varepsilon\,\theta \tag{7}$$

To generate the correct steering offset δ_t at the tip of the probe, the prescribed offset imposed at the base, δ, should be adjusted by $\Delta\delta$, as defined in (8).

$$\begin{aligned} \delta &= \delta_t + \Delta\delta \\ \delta_t &= \delta - \Delta\delta = \delta - \varepsilon\,\theta \end{aligned} \tag{8}$$

A modified kinematic model of the flexible probe which takes into account this adjustment is described in (9), where v_1 and v_2 indicate the forward velocity and the rate of change of steering offset (with the offset applied at the base of the probe), respectively. Please note that v_{t2} in (3) and v_2 in (9) are different quantities and that the shape of the trajectory does not affect the forward velocity v_1, which is considered here to be the forward motion of the middle point of the steering offset.

$$\begin{bmatrix} \dot{x} \\ \dot{y} \\ \dot{\theta} \\ \dot{\delta} \end{bmatrix} = \begin{bmatrix} \cos\theta \\ \sin\theta \\ \kappa(\delta - \varepsilon\,\theta) \\ 0 \end{bmatrix} v_1 + \begin{bmatrix} 0 \\ 0 \\ 0 \\ 1 \end{bmatrix} v_2 \tag{9}$$

Generally, the kinematic model of a non-holonomic system is nonlinear, as in (9), and can be expressed using the following equation:

$$\dot{q} = G(q)v \tag{10}$$

where q is a 4-vector of the flexible probe's generalized coordinates $[x, y, \theta, \delta]'$, v is a 2-vector of input velocities $[v_1, v_2]'$, and the columns g_i (i=1,2) of the 4×2 matrix $G(q)$ are vector fields [13].

III. Two-Dimensional Trajectory Following

A. Related Works and the Chained Form

In order to construct a feedback control algorithm for the probe, we adopt an algorithm developed for car-like robots (e.g. [13-16]), which has received significant attention over the years. One of the well-structured methods presented in the literature utilizes the chained form representation [13, 14, 16]. In this method, the bicycle model, which is similar to the one developed here for the flexible probe, can be converted into a "(2.4)" single chained form using new states ξ as in (11), with two input velocities, (v_1, v_2), and four states (x, y, θ, δ). By applying a similar approach to the one explained in [13], the kinematic model of the probe can then be converted into the chained form, as illustrated in (12). The function M converts the original coordinates q into the chained form's coordinates ξ. Equation (13) describes the function N, which converts the chained form's input $u = [u_1, u_2]'$ into the original input v.

$$\begin{aligned} \dot{\xi}_1 &= u_1 \\ \dot{\xi}_2 &= u_2 \\ \dot{\xi}_3 &= \xi_2 u_1 \\ \dot{\xi}_4 &= \xi_3 u_1 \end{aligned} \tag{11}$$

$$\xi = \begin{bmatrix} \xi_1 \\ \xi_2 \\ \xi_3 \\ \xi_4 \end{bmatrix} = \begin{bmatrix} x \\ \kappa(\delta - \varepsilon\theta)/\cos^3(\theta) \\ \tan(\theta) \\ y \end{bmatrix} = M(q) \tag{12}$$

$$v = \begin{bmatrix} \dfrac{1}{\cos\theta} & 0 \\ -\dfrac{3\kappa(\delta - \varepsilon\theta)^2 \sin\theta - \kappa\varepsilon(\delta - \varepsilon\theta)\cos\theta}{\cos^2\theta} & \dfrac{\cos^3\theta}{\kappa} \end{bmatrix} \begin{bmatrix} u_1 \\ u_2 \end{bmatrix} = N(q)u \tag{13}$$

Using the chained form to model the flexible probe, open- and closed-loop control become straightforward. First, based on a desired trajectory, open-loop or closed-loop input velocities can be computed using the chained form. Then, using (13), the inputs of the chained form can be converted back into the original inputs.

B. Open-Loop Control

Open-loop control implies the need to find input velocities to enable the probe to follow a predefined trajectory without access to feedback information. Given a desired trajectory as in (14), where σ is an intermediate trajectory parameter, the derivatives of the desired trajectories are obtained as in (15). By defining $\xi_{d1} = x_d$ and $\xi_{d4} = y_d$, the desired input for open-loop control can be obtained, as described in (16) [13]. In this case, the states of the probe will be as in (17). In this

application, the value $\dot{\sigma}(t)$ was utilized to keep the forward velocity v_{d1} constant using (16) and (18).

$$\begin{aligned} x_d &= x_d(\sigma(t)) \\ y_d &= y_d(\sigma(t)) \end{aligned} \tag{14}$$

$$\begin{aligned} \dot{x}_d(t) &= \frac{d}{dt}x_d(t) = \frac{dx_d(\sigma)}{d\sigma}\frac{d\sigma}{dt} = x_d'(\sigma)\dot{\sigma}(t) \\ \dot{y}_d(t) &= \frac{d}{dt}y_d(t) = \frac{dy_d(\sigma)}{d\sigma}\frac{d\sigma}{dt} = y_d'(\sigma)\dot{\sigma}(t) \end{aligned} \tag{15}$$

$$\begin{aligned} u_{d1} &= x_d'(\sigma)\dot{\sigma}(t) \\ u_{d2} &= \frac{x_d'^2 y_d''' - x_d' x_d''' y_d' - 3x_d' x_d'' y_d'' + 3x_d''^2 y_d'}{x_d'^4}\dot{\sigma}(t) \end{aligned} \tag{16}$$

$$\begin{aligned} \xi_{d1} &= x_d \\ \xi_{d2} &= (x_d' y_d'' - x_d'' y_d')/x_d'^3 \\ \xi_{d3} &= y_d'/x_d' \\ \xi_{d3} &= y_d \end{aligned} \tag{17}$$

$$v_{d1}(t) = \pm\sqrt{\dot{x}_d^2(t) + \dot{y}_d^2(t)} = \pm\sqrt{x_d'^2(\sigma) + y_d'^2(\sigma)}\dot{\sigma}(t) \tag{18}$$

C. Closed-Loop Control

De Luca *et al.* produced a feedback controller for trajectory tracking through approximate linearization [13]. This approach utilizes the state and input errors, which are denoted as in (19), to obtain the time-varying state space form.

$$\begin{aligned} \tilde{\xi}_i &= \xi_{di} - \xi_i, \qquad i = 1,\ldots,4 \\ \tilde{u}_j &= u_{dj} - u_j, \qquad j = 1,2 \end{aligned} \tag{19}$$

The chained form can be represented as the nonlinear error equations in (20).

$$\begin{aligned} \dot{\tilde{\xi}}_1 &= \tilde{u}_1 \\ \dot{\tilde{\xi}}_2 &= \tilde{u}_2 \\ \dot{\tilde{\xi}}_3 &= \xi_{d2}u_{d1} - \xi_2 u_1 = u_{d1}\tilde{\xi}_2 - \xi_2\tilde{u}_1 \\ \dot{\tilde{\xi}}_4 &= \xi_{d3}u_{d1} - \xi_3 u_1 = u_{d1}\tilde{\xi}_3 - \xi_3\tilde{u}_1 \end{aligned} \tag{20}$$

With the approximation $\xi_2 = \xi_{d2}$ and $\xi_3 = \xi_{d3}$, (20) can be converted to the linear state-space representation as in (21).

$$\begin{aligned} \dot{\tilde{\xi}} &= \begin{bmatrix} 0 & 0 & 0 & 0 \\ 0 & 0 & 0 & 0 \\ 0 & u_{d1}(t) & 0 & 0 \\ 0 & 0 & u_{d1}(t) & 0 \end{bmatrix}\tilde{\xi} + \begin{bmatrix} 1 & 0 \\ 0 & 1 \\ \xi_{d2}(t) & 0 \\ \xi_{d3}(t) & 0 \end{bmatrix}\tilde{u} \\ &= A(t)\tilde{\xi} + B(t)\tilde{u} \end{aligned} \tag{21}$$

where $\tilde{\xi} = \begin{bmatrix} \tilde{\xi}_1 & \tilde{\xi}_2 & \tilde{\xi}_3 & \tilde{\xi}_4 \end{bmatrix}'$ and $\tilde{u} = \begin{bmatrix} \tilde{u}_1 & \tilde{u}_2 \end{bmatrix}'$. If input errors are defined as in (22), the closed-loop dynamics of the probe become as in (23), with the characteristic polynomial (24), the eigenvalues of which can be easily manipulated.

$$\begin{aligned} \tilde{u}_1 &= -k_1\tilde{\xi}_1 \\ \tilde{u}_2 &= -k_2\tilde{\xi}_2 - \frac{k_3}{u_{d1}}\tilde{\xi}_3 - \frac{k_4}{u_{d1}}\tilde{\xi}_4 \end{aligned} \tag{22}$$

$$A_{cl}(t) = \begin{bmatrix} -k_1 & 0 & 0 & 0 \\ 0 & -k_2 & -k_3/u_{d1} & -k_4/u_{d1}^2 \\ -k_1\xi_{d2} & u_{d1} & 0 & 0 \\ -k_1\xi_{d3} & 0 & u_{d1} & 0 \end{bmatrix} \tag{23}$$

$$\det(\lambda I - A_{cl}) = (\lambda + k_1)(\lambda^3 + k_2\lambda^2 + k_3\lambda + k_4) \tag{24}$$

The overall control input to the chained form is thus:

$$u = u_d - \tilde{u}\,. \tag{25}$$

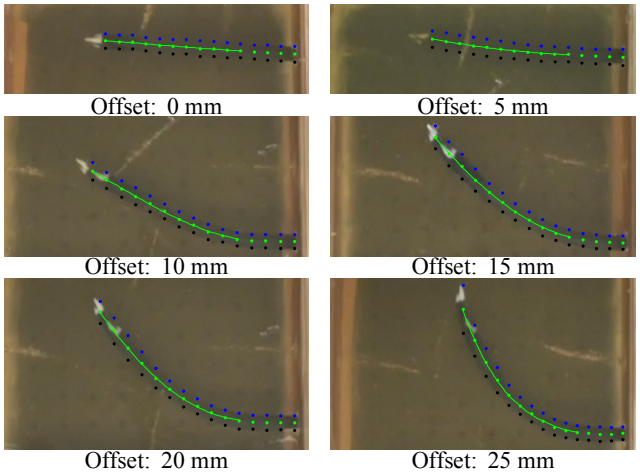

Fig. 4. Still images of the flexible probe with various steering offsets.

IV. Simulation and Experimental Calibration

A. Steering Offset vs. Curvature Calibration

In (2), it was assumed that the curvature would be a function of the steering offset. To investigate this relationship, a set of experiments was performed using a first prototype with 12 mm diameter, manufactured with rapid prototyping (RP) techniques in a rubber-like material (TangoBlack – FullCure 970, Objet; tensile strength of 2MPa; hardness of 61 Shore Scale A; elongation at break of 48%) [11]. A 6 wt. % gelatin phantom, with a mixture of 1.3 ml of gelatin to 20ml of boiling water, was used in these experiments, as this solution at 20~21ºC is reported to nearly duplicate the resistance of *in vitro* canine brain at 38ºC [17]. A custom-made trocar, with 12.5mm inner diameter, was introduced to eliminate the possibility of buckling outside of the gelatin phantom. Six tests were performed, where the steering offset varied from 0mm to 25mm at 5mm intervals. Each trajectory was captured using a video camera (Sony Handycam HDR-SR10E) from a top-down view. Each image was calibrated using key reference points (i.e. the size of the gelatin box), then the shape of the probe was manually measured on each frame of the video capture as shown in Fig. 4. Given the relatively small influence of out of plane deviations of the measured trajectories on the scaling coefficient κ, off-plane errors in this set of experiments were neglected for the sake of simplicity.

In order to extract curvature information from the experimentally acquired points, a 4th-order polynomial fit ($0.9927 \le R^2 \le 0.9999$) was used on the raw image data (green lines in Fig. 4). Curvature values for increasing insertion depths were then computed, as illustrated in Fig. 5a. Fig. 5b shows the average curvature recorded for each steering offset.

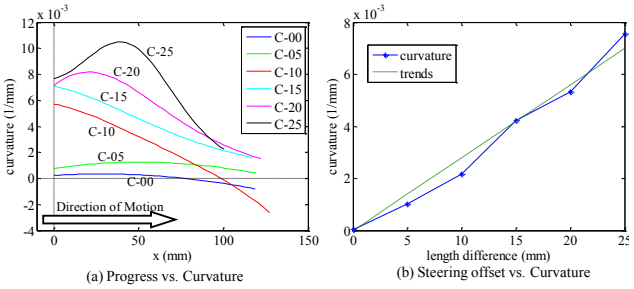

(a) Progress vs. Curvature (b) Steering offset vs. Curvature

Fig. 5. Measured curvature according to different steering offsets.

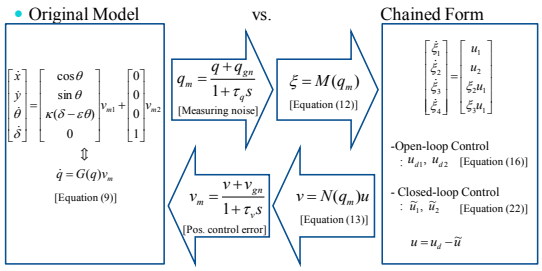

Fig. 6. Flow chart of simulation using the chained form.

Based on these results, the curvature was found to be approximately proportional to the steering offset, with a coefficient $\kappa = 2.80 \times 10^{-4} (mm^{-2})$.

B. Steering Offset Compensation

The compensation coefficient ε in (7) was determined theoretically as twice the distance from the center to the centroid of each valve [18]. ε for a probe with two halves is thus $(8R)/(3\pi)$, and with four quarters is $(8\sqrt{2}R)/(3\pi)$.

C. Simulation

In this section, a simulation of the flexible probe's performance when controlled via the chained form representation is presented. The general sequence of the simulation is shown in Fig. 6. First, Gaussian measurement noise (q_{gn}) is added to the current states of the probe (q) in order to mimic disturbances in the EM tracker measurements [19] which will relay information about the tip of the flexible probe once real experiments on a functional prototype are performed. These measured states (q_m) are used to obtain the states (ξ) of the chained form. Inputs (u) are then converted back into the input velocities (v) from the chained form, followed by the addition of velocity control noise (v_{gn}). Finally, an input velocity (v_m) is applied to simulate the behavior of the probe. TABLE 1 lists all parameters considered in this simulation.

TABLE 1. USED PARAMETERS FOR TRAJECTORY FOLLOWING SIMULATION

Parameters		Values
Trajectory	Equation	(26)
	A, L	15mm, 150mm
Exact initial posture	$[x_0, y_0, \theta_0, \delta_0]'$	[0mm, 0mm, 0°, 11.75mm]'
Init. posture disturb.	$[x_0, y_0, \theta_0, \delta_0]'$	[0mm, 1mm, 2°, 11.75mm]'
Measurement noise	$[x_{gn}, y_{gn}, \theta_{gn}, \delta_{gn}]'$	[0.9mm, 0.9mm, 0.3°, 0.5mm]'
Control noise	$[v_{gn1}, v_{gn2}]'$	[0.5mm/s, 0.5mm/s]'
Linear velocity	v_{d1}	1 mm/s
Steering coeff.	κ	0.000280 mm^{-2}
Compensation coeff.	ε	7.20 mm
Time constant	τ_q, τ_v	0.2s, 0.2s
Control gain	$[k_1, k_2, k_3, k_4]$	[0.1, 0.2, 0.02, 0.001]

$$x_d(\sigma) = \sigma$$
$$y_d(\sigma) = \frac{A}{2}\left(1 - \cos\left(\frac{\pi}{L}\sigma\right)\right) \qquad (26)$$

V. Result & Discussion

Fig. 7 shows the simulation results obtained for the kinematic model of our flexible probe. Fig. 7a shows the simulation results for open-loop control with an exact initial posture; Fig. 7b shows the results of open-loop control with an initial posture perturbation; Fig. 7c shows the results of closed-loop control, which employs both the feed-forward and the feedback terms, with an initial posture perturbation equivalent to that in Fig. 7b.

These simulation results show that the kinematic model and control strategy implemented for our flexible probe with a programmable bevel tip work as expected. Open-loop control results show near perfect trajectory following capabilities in the absence of noise and initial posture perturbation, the introduction of which quickly deteriorates tracking performance.

In contrast, the closed-loop control simulation results show good convergence after 40mm motion, as shown in Fig. 7c. The maximum error after convergence was measured to be less than 0.3mm ($e_{max} < 0.3$, $x > 40$). Indeed, faster convergence would be possible if larger eigenvalues were chosen (for these results, eigenvalues were set to $[-0.1, -0.1, -0.05(1 \pm i\sqrt{3})]$). However, considering the probe's dynamics and desired forward velocity are slow, these eigenvalues were deemed appropriate. In addition, since

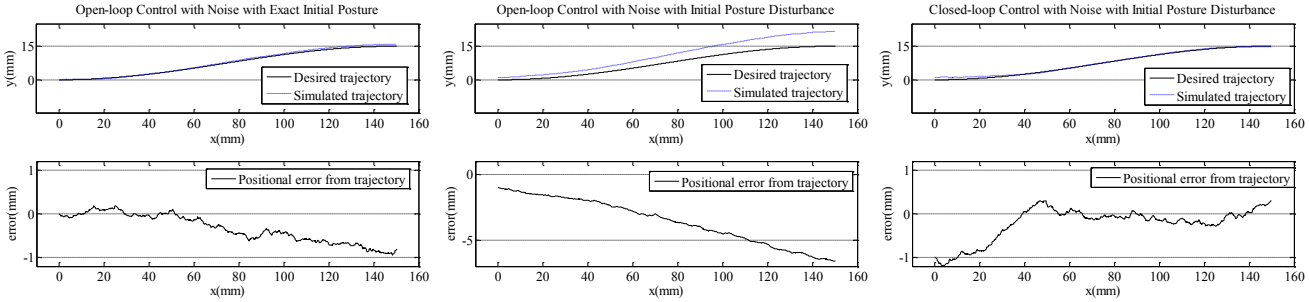

(a) Open-loop control with exact initial posture (b) Open-loop control with initial posture disturbance (c) Closed-loop control with initial posture disturbance

Fig. 7. Simulation results with flexible probe.

closed-loop control can minimize the effect of uncertainty and external disturbances, it is expected that our flexible probe will mitigate the positional error introduced by, for example, an inaccurate coefficient κ between the steering offset and the curvature, and/or small perturbations in the initial insertion position.

In the simulations, a first-order low pass filter with time constant of 0.2sec was utilized to reduce the effect of measurement noise. Since the probe moves slowly (i.e. approximately 1mm/sec or less), the delay introduced by the filtering process is negligible.

Two limitations affect the definition of a trajectory for the control method described here. First, the trajectory needs to be differentiable three times to ensure that the feed-forward inputs in (16) can be computed. Second, the trajectory as described here can never be parallel to the y-axis, since x'_d would become zero and u_{d2} infinity. Considering the probe's maximum curvature and intended application, such limitations are acceptable.

VI. Conclusion & Future Work

This paper describes on-going research into the control of a bio-inspired flexible probe. Based on the characteristics of certain ovipositing wasps, the concept of a "programmable bevel" was proposed to steer the probe in a predefined direction: the offset between probe segments determines the steering direction of the tip thanks to a set of bevels placed at the tip of each segment. A kinematic model of the probe was derived, based on its similarity to that of car-like robots. In this research, the instantaneous curvature of the probe is assumed to be a function of the steering offset, which is shown to be proportional to the steering offset through a simple set of experimental trials in gelatin. A compensation algorithm to account for differences in steering offset between base and tip coordinates was also proposed. Finally, open-loop (feed-forward) and closed-loop (feedback) control strategies for two-dimensional path following were implemented using the chained form representation. Simulation results demonstrate that both the kinematic model and control methods implemented for the probe perform as expected.

Though these early simulation results are promising, research to date offers significant scope for future work. An experimental verification of the feedback control algorithm described, with a 12mm prototype of the flexible probe, is currently underway. In addition, we currently assume that there is no friction between probe segments and that the probe is very flexible, while being stiff in compression and in tension. However, experiments to date on the prototype show that such assumptions may be overoptimistic, which means that further improvements to the kinematic model are needed. Next, both the kinematic model and control schemes described here will be extended to three-dimensions. Finally, probe miniaturization will need to be studied intensively to ensure that this approach becomes clinically viable. A substantial decrease in the probe's outer diameter is also expected to increase the steering capabilities of the probe (i.e. produce a larger κ), further extending the range of potential clinical applications for the probe.

References

[1] N. Abolhassani, R. Patel, and M. Moallem, "Needle insertion into soft tissue: A survey," *Medical Engineering & Physics,* vol. 29, pp. 413–431, 2007.

[2] S. P. DiMaio and S. E. Salcudean, "Needle Steering and Model-Based Trajectory Planning," in *MICCAI*, 2003.

[3] D. Glozman and M. Shoham, "Flexible Needle Steering and Optimal Trajectory Planning for Percutaneous Therapies," *Lecture Notes in Computer Science,* vol. 3217, pp. 137-144, 2004.

[4] R. J. Webster III, J. S. Kim, N. J. Cowan, G. S. Chirikjian, and A. M. Okamura, "Nonholonomic Modeling of Needle Steering," *The International Journal of Robotics Research,* vol. 25, pp. 509-525, May-June 2006.

[5] R. Alterovitz, M. Branicky, and K. Goldberg, "Motion Planning Under Uncertainty for Image-guided Medical Needle Steering," *The International Journal of Robotics Research,* vol. 27, pp. 1361-1374, November 1 2008.

[6] K. B. Reed, A. M. Okamura, and N. J. Cowan, "Modeling and Control of Needles with Torsional Friction," *IEEE Transactions on Biomedical Engineering,* vol. 56, pp. 2905-2916, 2009.

[7] V. Kallem and N. J. Cowan, "Image Guidance of Flexible Tip-Steerable Needles," *IEEE TRANSACTIONS ON ROBOTICS,* vol. 25, pp. 191-196, February 2009.

[8] D. S. Minhas, J. A. Engh, M. M. Fenske, and C. N. Riviere, "Modeling of Needle Steering via Duty-Cycled Spinning," in *the 29th Annual International Conference of the IEEE EMBS*, Lyon, France, 2007, pp. pp. 2756-2759.

[9] D. Glozman and M. Shoham, "Image-Guided Robotic Flexible Needle Steering," *IEEE TRANSACTIONS ON ROBOTICS,* vol. 23, pp. 459-467, June 2007.

[10] K. B. Reed, V. Kallem, R. Alterovitz, K. Goldberg, A. M. Okamura, and N. J. Cowan, "Integrated Planning and Image-Guided Control for Planar Needle Steering," in *IEEE/RAS-EMBS International Conference on Biomedical Robotics and Biomechatronics*, Scottsdale, AZ, USA, 2008.

[11] L. Frasson, S. Y. Ko, A. Turner, T. Parittotokkaporn, B. L. Davies, J. F. Vincent, and F. Rodriguez y Baena, "STING: a soft-tissue intervention and neurosurgical guide to access deep brain lesions through curved trajectories," *Proc. IMechE Part H: J. Engineering in Medicine,* vol. 223, 2009.

[12] L. Frasson, S. Reina, B. L. Davies, and F. M. Rodriguez y Baena, "Design Optimization of a Biologically Inspired Multi-Part Probe for Soft Tissue Surgery," in *11th International Congress of the IUPESM, Medical Physics and Biomedical Engineering*, Munich, German, 2009, pp. 307–310.

[13] A. De Luca, G. Oriolo, and C. Samson, "Feedback Control of a Nonholonomic Car-like Robot " in *Robot Motion Planning and Control*, J. P. Laumond, Ed.: Springer, 1998, pp. 172-253.

[14] C. Samson, "Control of Chained Systems Application to Path Following and Time-Varying Point-Stabilization of Mobile Robots," *IEEE Transactions on Automatic Control,* vol. 40, pp. 64-77, January 1995.

[15] D. J. Cole, A. J. Pick, and A. M. C. Odhams, "Predictive and linear quadratic methods for potential application to modelling driver steering control," *Vehicle System Dynamics,* vol. 44, pp. 259–284, March 2006.

[16] Y. Tan, Z. Jiang, and Z. Zhou, "A Nonholonomic Motion Planning and Control Based on Chained Form Transformation," in *IEEE/RSJ International Conference on Intelligent Robots and Systems*, Beijing, China, 2006, pp. 3149 - 3153.

[17] R. C. Ritter, E. G. Quate, G. T. Gillies, M. S. Grady, M. A. Howard III, and W. C. Broaddus, "Measurement of Friction on Straight Catheters in *in vitro* Brain and Phantom Material," *IEEE Transactions on Biomedical Engineering,* vol. 45, pp. 476-485, April 1998.

[18] E. J. Hearn, *Mechanics of materials. 1, An introduction of the mechanics of elastic and plastic deformation of solids and structural materials*, 3rd ed. ed. Oxford: Butterworth-Heinemann, 1997.

[19] Northern Digital Inc., (2010, Feb 19), Available: http://www.ndigital.com/